frontiers in Earth Science

BRIEF RESEARCH REPORT
published: 11 June 2020
doi: 10.3389/feart.2020.00189

Plio-Pleistocene Dust Traps on Paleokarst Surfaces: A Case Study From the Carpathian Basin

János Kovács[1,2]*, *Gábor Újvári*[3,4], *György Varga*[5], *Klemens Seelos*[6], *Péter Szabó*[1,2], *József Dezső*[7] and *Nadia Gammoudi*[1]

[1] Department of Geology and Meteorology, University of Pécs, Pécs, Hungary, [2] Environmental Analytical and Geoanalytical Research Group, Szentágothai Research Centre, University of Pécs, Pécs, Hungary, [3] Department of Lithospheric Research, University of Vienna, Vienna, Austria, [4] Institute for Geological and Geochemical Research, Research Centre for Astronomy and Earth Sciences, Budapest, Hungary, [5] Geographical Institute, Research Centre for Astronomy and Earth Sciences, Budapest, Hungary, [6] Institute of Geosciences, Johannes Gutenberg University Mainz, Mainz, Germany, [7] Department of Physical and Environmental Geography, University of Pécs, Pécs, Hungary

Plio-Pleistocene silt/clay-rich deposits and paleo-karst fissure sediments from sites of the northern and southern parts of the Carpathian Basin were investigated. These materials were supposed to be mixed during transport before being captured in karstified fissures. Evidence that the eolian fissure sediments of Plio-Pleistocene age in the older Triassic–Cretaceous limestones are derived from eolian silt and clay includes compositional and textural matches, especially decreasing grain-size trends observed downwards from the paleo-surface of the former landscape. Various environmental factors could be recognized by the statistical evaluation of grain-size distribution curves of fissure fillings sediments, such as the effects of eolian transport, parent rock type, weathering, and other sediment transport processes. Grain-size distribution curves with a single maximum in the silt size range are typical for the overlying siltstone debris, for the redeposited loess and red paleosol underlying the loess. Red clay fissure fillings yield bimodal grain-size distribution curves with maxima both in the clay and silt fractions. The research reported in this paper identifies for the first time the presence of eolian deposits in karst fissures of the Carpathian Basin and investigates the characteristics and origin.

Keywords: eolian sedimentation, clay, paleosol, karst, Pliocene, Pleistocene, Carpathian basin

OPEN ACCESS

Edited by:
Davide Tiranti,
Agenzia Regionale per la Protezione Ambientale (ARPA), Italy

Reviewed by:
Qiang Jin,
China University of Petroleum (Huadong), China
Andrea Zerboni,
University of Milan, Italy

***Correspondence:**
János Kovács
jones@gamma.ttk.pte.hu

Specialty section:
This article was submitted to Quaternary Science, Geomorphology and Paleoenvironment, a section of the journal Frontiers in Earth Science

Received: *19 March 2020*
Accepted: *12 May 2020*
Published: *11 June 2020*

Citation:
Kovács J, Újvári G, Varga G, Seelos K, Szabó P, Dezső J and Gammoudi N (2020) Plio-Pleistocene Dust Traps on Paleokarst Surfaces: A Case Study From the Carpathian Basin. Front. Earth Sci. 8:189. doi: 10.3389/feart.2020.00189

INTRODUCTION

Granulometry based on laser diffraction is a fundamental technique widely used in eolian sediment research (Tsoar and Pye, 1987). Substantial accumulations of silty wind-blown dust require a source of silt and clay particles, transport media (prevalent winds of adequate energy), climate, and sediment traps (Tsoar and Pye, 1987; Evans and Reed, 2007; Kok et al., 2012; Újvári et al., 2016). The rate and distance of eolian transportation strongly depend on grain ability and availability (grain-size and shape), terrain and wind strength (Evans and Reed, 2007; Varga et al., 2011; Kok et al., 2012; Vandenberghe, 2013; Újvári et al., 2016). Allochthonous karst depression, cave and fissure-fill sediments are mostly believed to be originated from local sources (Pickford and Mein, 1988; Atalay, 1997; Evans and Reed, 2007; Peresani et al., 2008; Evans and Soreghan, 2015; Muttoni et al., 2017), and considered to be derived from the terrain directly overlying the fracture networks on carbonates (Bosch and White, 2007; Costantini et al., 2009; Mikulčić Pavlaković et al., 2011; Gil et al., 2013; Al-Farraj et al., 2014; Peng et al., 2019; Soriano et al., 2019). Only a few studies have

recognized the link between cave and fissure sediments and wind-blown dust (Coude-Gaussen et al., 1984; Villa et al., 1995; Evans and Reed, 2007; Merino and Banerjee, 2008; Rellini et al., 2013; Evans and Soreghan, 2015; Andreucci et al., 2017; Kovács et al., 2017; Bosák and Zupan Hajna, 2018; Durn et al., 2018; Ge et al., 2020). As stated by Musgrave and Webb (2004), Merino and Banerjee (2008) the reddish terra rossa and other cave sediments on carbonates are mostly originated from mineral dust. Evans and Soreghan (2015) found that the "wind-driven deposits in karst fissures and subterrane networks are sole data provider of continental-scale information about local and distant source areas, land-atmosphere transfer processes, surface depositional processes, erosion, transport, and resedimentation into karst networks." The physics of silt and clay particle mobilization, transport and deposition are discussed in detail by Újvári et al. (2016). Since grains bigger than 20 μm are generally transported by low-level winds, dust trapping is more effective in the leeward of topographic obstacles (Tsoar and Pye, 1987; Evans and Reed, 2007). The accumulated eolian dust may be reactivated by wind or wore away by surface and subsurface (groundwater) water which can be a key process of sediment redistribution (Bal and Buursink, 1976). The red siliciclastic (clay/silt) deposits of the Carpathian Basin are recognized from both exposures and boreholes (Fekete, 2002, 2014; Viczián, 2002, 2011; Kovács, 2008; Kovács et al., 2011, 2013). Previous work identified the red clays in the Carpathian Basin as a variety of loess, sediment formed by the deposition of wind-borne silt or formed by the weathering of volcanic material or even as a bauxite related sediment (Kovács, 2008 and references therein). The eolian origin of the Plio-Pleistocene red clay in the Carpathian Basin was proposed by Kovács (2008). The provenance of dust found in red clay and loess in the region is a source of considerable debate (Kovács, 2008; Újvári et al., 2010, 2012). As highlighted by Kovács (2008) and Újvári et al. (2012), earlier researches "described glacial sources for the loess to the north-northwest of the Carpathian Basin, while others inferred a dominantly local source for the loess and red clay such as Miocene flysch and molasse, Miocene–Pliocene sands." According to Smalley et al. (2009), loess was originating from the Alps, Carpathians, and Sudeten. Recent works based on geochemistry and loess accumulation rates identify mountain sources such as the Alps and the Carpathians (Buggle et al., 2008; Újvári et al., 2010; Stevens et al., 2011; Marković et al., 2015). A recent dust provenance study based on clay mineralogy, Sr-Nd isotopes and zircon U-Pb ages by Újvári et al. (2012) suggest that "the Danube loess in the Carpathian Basin was derived from two major sources: alluvial fans of the Danube River and local rocks exposed in the surrounding mountains of specific loess sites." A North African influence as a source of fine dust in red clays and loess is unlikely based on clay mineralogical and granulometric considerations (Újvári et al., 2012; Kovács et al., 2013). This research aimed at better understanding the origin of Upper Pliocene and Pleistocene allochthonous fissure deposits in Triassic and Cretaceous limestones in the Carpathian Basin (Kovács et al., 2017). These fissure deposits can be linked to the overlying silty (loessic) deposits, with long-distance (Alpine realm, Western Europe, Carpathian foreland) or short-distance (Carpathian Basin) source areas (Újvári et al., 2010, 2012; Kovács et al., 2013; Marković et al., 2015; Obreht et al., 2019).

SAMPLING SITES

The sampling sites in Hungary and Slovakia were chosen according to their geological and geographical settings (**Figure 1**). As stated in Újvári et al. (2010), "diverse eolian accumulation and sedimentation are expected under different physiographic situations." All sites are karst areas on Triassic and Cretaceous limestones and situated in the Danube loess belt (Marković et al., 2015). The two sites in Slovakia are on the foothills of the Carpathians while the Hungarian sites are in a low-elevated hilly region in the southern part of the basin, far away from the Alps and the Carpathians (**Figure 1**).

Beremend Limestone Quarry (Hungary)

Beremend site is located 10 km south from the Villány Hills and the city of Villány, in Southern Hungary (**Figure 1C**). The flat limestone hill is covered by loess-paleosol succession and its altitude is 174 m. Pliocene-Pleistocene mammalian faunas were discovered from the karst cavities (with red clay infilling) of Lower Cretaceous limestone (Pazonyi et al., 2016). This carbonate rock suite (Nagyharsány Limestone) is a 400–500 m thick Urgon facies limestone (Császár, 2002). The karst processes of the area are described in detail by Erőss et al. (2020).

Csarnóta Limestone Quarry (Hungary)

This site is found at Cser Hill, about 1.5 km south from the municipality of Csarnóta in the Villány Hills, in South Hungary (**Figure 1D**). Some parts of the quarry (Csarnóta 1–3) are typical red clay sequences which are fissure infills in Triassic limestone, while another part (Csarnóta 4) consists of reddish cave deposits (Jánossy, 1986). The Triassic limestone (Lapis Limestone) is 300 m thick with features similar to those of the "Wellenkalk" facies of the Germanic Triassic (Török, 1998). Based on mammalian fossils, the Csarnóta 1–3 fissure infills may have formed during the early Late Pliocene and are correlated with the MN 15-16A "Mammals Neogene" (MN) zones (Szentesi et al., 2015).

Ivanovce Limestone Quarry (Slovakia)

The Ivanovce locality (**Figure 1A**) was discovered by Fejfar (1961). The site is situated in western Slovakia ∼12 km south-west from the municipality of Trenčín. It consists of reddish silty clay sediment fill within horizontal and vertical karst fissures in tectonically deformed Triassic limestone (Bronger et al., 1984). Based on the micro-mammalian fauna, the age of sediments at this locality was assigned to the late Early Pliocene (Late Ruscinian, MN 15b) (Fejfar et al., 2012).

Včeláre Limestone Quarry (Slovakia)

The site is a limestone quarry situated in the south-eastern part of the Slovak Karst on the Dolny' Vrch Range, south of the village of Včeláre (**Figure 1B**). The quarry is opened on a Middle Triassic limestone with a network of karst fissures filled with terra rossa (red clay) sediments along with fragments of limestone. The

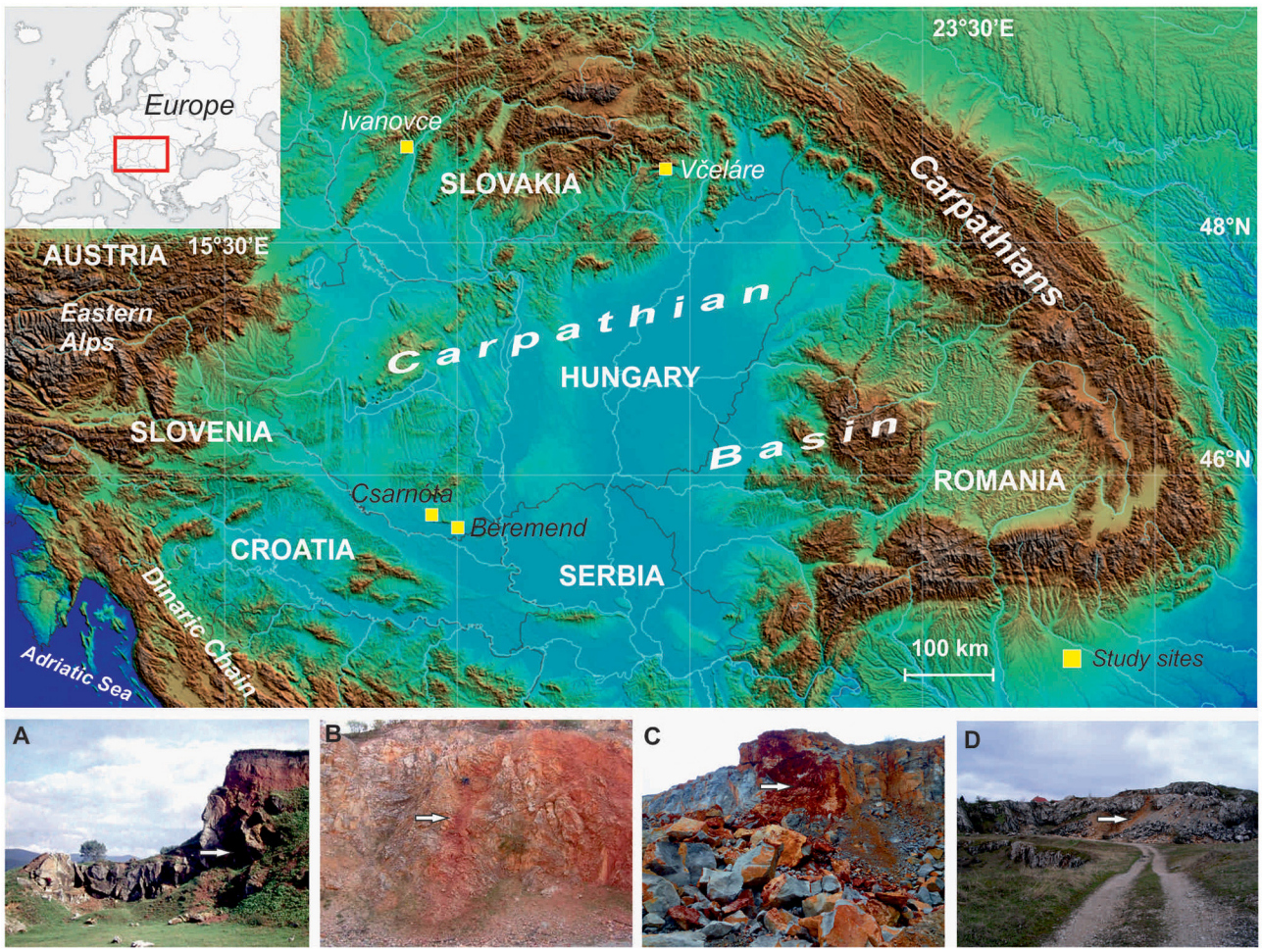

FIGURE 1 | Map of the study area in the Carpathian Basin. Study sites are: **(A)** Ivanovce; **(B)** Včeláre; **(C)** Beremend; **(D)** Csarnóta. The white arrows show the sampling points (Original map: DEM map of the Pannonian Basin, © Dept. of Geophysics, Eötvös University).

fissures are several meters wide and could also have been natural traps for various animals (Sabol et al., 2008). Fossil assemblages from Včeláre 3 represent a Villanyian fauna (Early Pleistocene, MN17), whereas the fossiliferous fissure fillings of the Včeláre 4 assemblage are dated to Early Biharian (mid-Pleistocene, MQ1) (Fejfar and Horáček, 1983).

METHODS

Sampling

At every site, well-developed vertical fissures (opening from the recent surface) was chosen for sampling. The fissures are not from deep karst systems. Kubiëna-type zinc boxes were used to collect undisturbed samples from the fissures for thin-section analyses. Disturbed samples for grain-size analysis were taken from the surroundings of the undisturbed sampling spots. The samples are from fine-grained, homogeneous units of the fissure fillings. The reddish sediments from the fissures were described as red clays and silts at every location, except for Včeláre, where the material was characterized as terra rossa.

Laser Diffraction Particle Sizing

Before the laser diffraction measurements, red clay samples ($n = 75$) were pretreated with (10 ml, 30%) H_2O_2 to oxidize the organic material and (10 ml, 10%) HCl to remove the carbonate, 10 ml of 3.6% $Na_4P_2O_7 \cdot 10H_2O$ was added to disperse particles (Konert and Vandenberghe, 1997; Kovács, 2008; Újvári et al., 2016). Grain-size of the samples was made using a Malvern Mastersizer 3000 laser scattering device. With the wet dispersion unit (Hydro LV), particle size distributions are given as volume percentage of particles classed into 101 logarithmically distributed (log-spaced) size bins from 0.01 to 2,100 μm (Varga et al., 2018, 2019). Laser light scattering features of this instrument are discussed in detail in Varga et al. (2018, 2019). In this study, values of 1.54 for the refractive index and 0.1 for the absorption coefficient (1.54-i0.1) were applied, while 1.33 for the refractive index was used for the dispersant water. Reported refractive indices of soil-forming minerals generally fall within a relatively narrow range, in overlap with the value adopted in this study (Varga et al., 2018, 2019). However, the exact value of the absorption coefficient is also dependent on

particle shape and surface roughness beside the mineralogical composition (Varga et al., 2018, 2019). As stated by Varga et al. (2019), "to get an overview on the effects of optical settings on particle size distributions, sensitivity tests were made with the combination of various refractive indices (Ri: 1.45–1.6) and absorption coefficients (Ac: 0.01–1)."

RADIUS—Rapid Particle Analysis of Digital Images

The particle analysis method RADIUS [Rapid Particle Analysis of digital Images by ultra-high-resolution scanning of thin sections, Seelos and Sirocko (2005)] was developed to analyze and identify the different sediment structures in sediment cores (Sirocko et al., 2005). "This method allows the detection of climate-controlled sedimentation processes like storm events under cold and dry conditions or fine laminated sequences related to warm periods, as well as spontaneous events such as volcanic eruptions, slumps and turbidities" (Seelos et al., 2009). The procedure is based on digital image analysis of single particles in a 200 μm interval. Each measurement provides a set of particle size and shape parameters like ECD (Equivalent Circle Diameter), perimeter, elongation, and roundness (surface roughness). The detection limit is around 2 μm. In this study, the thin sections were scanned with 20× magnification under cross-polarized light. Digital image analysis does not allow measuring and specifying PSDs as a percentage by weight but as an area ratio.

Heavy Mineral Separation

For quantitative heavy mineral analysis, the samples were treated with diluted HCl (10%) and ultrasonic agitation to eliminate the carbonates while iron coatings were removed by oxalic acid. The 0.040–125 mm size fraction was studied because it is the most representative overview of the bulk sample. The heavy mineral fraction (HMF) was separated using fast float liquid (methylene iodide, CH_2I_2) at a density of 3.32 g mL^{-1}. Lastly, a Frantz L-1 magnetic separator was used to remove the paramagnetic minerals. The HMFs (250–300 grains) were examined in reflected and transmitted light (Nikon Eclipse E600POL) microscopy for qualitative and semi-quantitative analysis and the percentage of each mineral was calculated following the method of Mange and Maurer (1992).

Statistics

Grain-size distribution curves of laser diffraction measurements were partitioned by parametric curve-fitting (Equation 1). The polymodal size distributions were separated into three unimodal Weibull-functions, and this way the measured grain-size distribution can be interpreted as a sum of these functions representing three sediment populations.

$$GSD = \sum_{i=1}^{3} W_i = c_i \times \left(\frac{\alpha_i}{\beta_i^{\alpha_i}}\right) \times x^{\alpha_i - 1} \times e^{-\left(\frac{x}{\beta_i}\right)^{\alpha_i}} \quad (1)$$

Here, the shape (α_i), location (β_i) and weighting (c_i) parameters of the three Weibull-functions were modified by an iterative numerical method as a least-squares problem by assessing the goodness of fit of measured data and calculated size distributions of constructed subpopulations (Varga et al., 2019).

RESULTS AND DISCUSSION

Radius

A representative sample (BER3, **Figure 2** first column) from the Beremend site (**Figure 1C**) was chosen to demonstrate RADIUS results. This 50 mm long thin-section image has a maximum resolution of 2 μm in particle-diameter. The thin-section sample is vertically oriented to the depositional process. In theory, it is possible to detect clay particles at this resolution. In practice, luckily, the clay/fine silt fractions in the sample have specific colors that allow a precise detection by color separation.

The amount of four different sedimentary phases is shown in the second column (**Figure 2A**). The upper part of the sample is characterized by a quartz content of ∼10% embedded in brownish and red clay/fine silt. The amount of red clay increases significantly up to 80% in the lower part of the section. At the same time, the quartz content decreases but remains visible. The abundance of Fe-Mn stains seems to co-vary with the content of red clay. **Figure 2B** shows the mean values of particle roundness/elongation: the curves are stable from top to bottom of the section—an indication of sediment homogeneity. The dataset demonstrates that the roundness of quartz is not influenced by and linked with brownish/red clay content. The particle size distribution curve for quartz (**Figure 2D**) shows the same. So, quartz particle size distributions seem to be independent of the clay fractions implying that it is not transported together with the clay fractions over longer distances. The quartz grains are from proximal, the silt/clay particles are from more distal sources. Looking at particle sizes of quartz (**Figure 2C**), the smooth curve of the mean values (being in a narrow range from 40 to 50 micron) suggests one transport mechanism. These grain-size values are typical for loess sediments. The sediments are well-sorted, which is seen in **Figure 2D**: lines showing the inner 50% (between percentile 25 and 75) are close to each other, implying symmetrical and narrow distributions as indicators of eolian sediments.

Grain-Size Analyses

The grain-size distributions were found to be diverse, with the majority of sedimentary particles falling into the medium and coarse silt-sized fractions to fine sands, and with a considerable volumetric contribution of clay and fine-silt fractions. Curve-fittings provided exceptionally high correlation coefficients ($r^2 > 0.99$), indicating a proper fitting of parametric distribution functions to the complex grain-size curves (**Figure 3**). The fitted unimodal distribution functions covered the whole spectrum of the measured size fractions. Modal grain-sizes of W_1 populations were relatively stable around ∼4.5–5 μm, while size maxima of the W_2 (medium and coarse silt-sized fractions) and W_3 (fine sand dominated fraction) populations display a more varied picture with values scattering between ∼20 and 90 μm, and ∼95 and 300 μm, respectively. In all cases, a volumetric proportion of W_2 or W_3 populations were recorded as the highest ones. The presented grain-size data and the results of

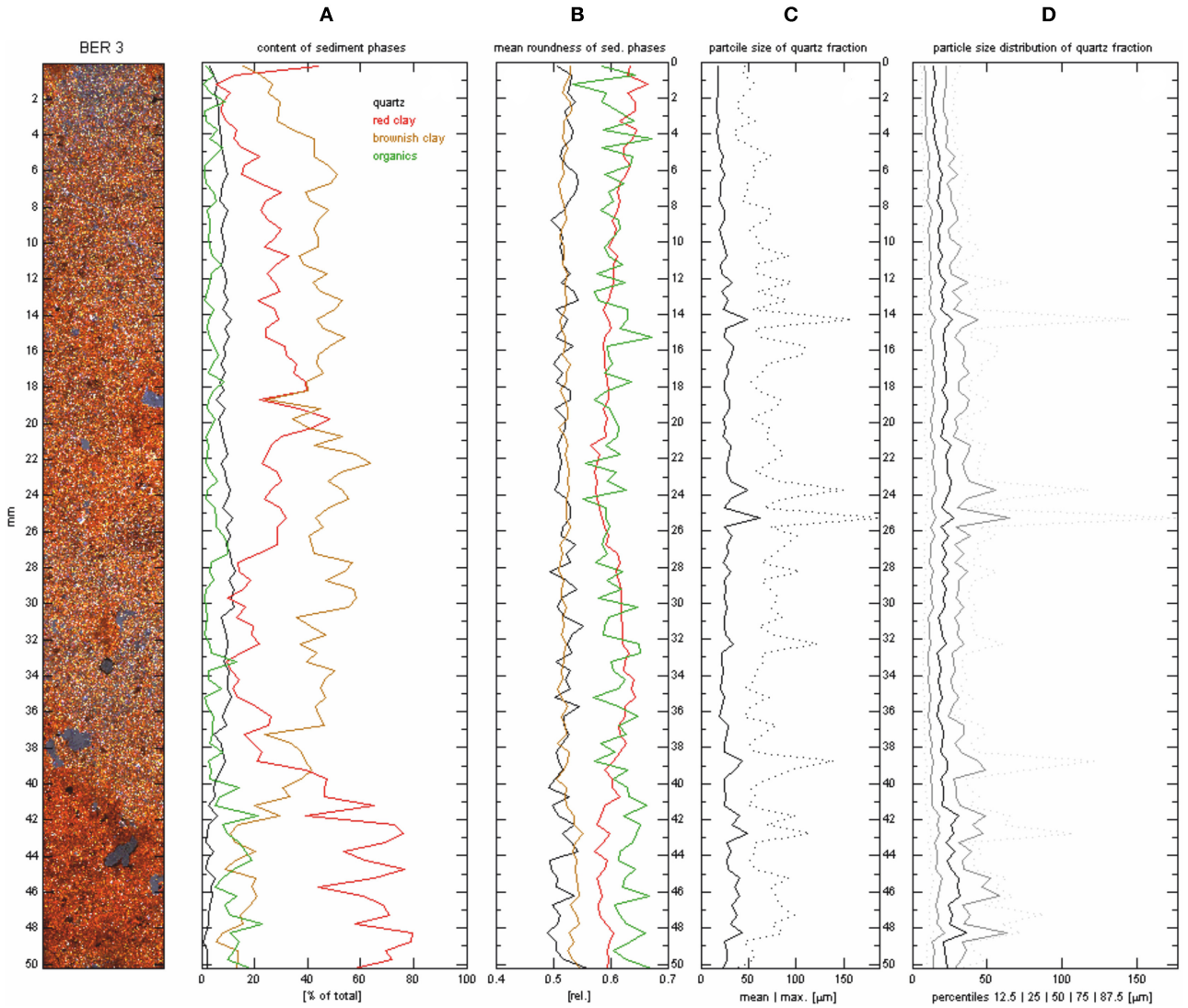

FIGURE 2 | The RADIUS detection system of red clay samples from fissure BER (Beremend, see in **Figure 1C**). **(A)** Content of sediment phases; **(B)** Mean roundness of sediment phases; **(C)** Particle size of quartz fraction; **(D)** Particle size distribution of quartz fraction.

subpopulation separations reveal that all of the investigated sedimentary materials were deposited in complex and relatively dynamic sedimentary environments. However, by removing the W_3 populations, we can concentrate only on the W_1 and W_2 groups. This way the majority of grain-size distribution curves have uniform shape patterns with definite positive skewness (asymmetry into the direction of coarse fractions), unimodality (or weakly developed bimodality), leptokurtic kurtosis and dominant appearance of medium and coarse silt-sized subpopulations. All of these characteristics are fairly similar to those of eolian loess-paleosol deposits and suggest a strong influence and admixture of windblown dust (Sun et al., 2002, 2004; Vandenberghe, 2013; Vandenberghe et al., 2018; Varga et al., 2019). Moreover, the above-mentioned characteristics are in good agreement with the Plio-Pleistocene red silt/clay sediment in the Carpathian Basin (Kovács, 2008; Kovács et al., 2008, 2011, 2013).

Heavy Mineral Composition

The heavy mineral spectra of the samples are as follows: amphibole, apatite, corundum, epidote, garnet, kyanite, monazite, pyroxene, rutile, spinel, staurolite, titanite, tourmaline, and zircon (**Figure 4**). Garnet (28–29%), amphibole (25–26%), and pyroxenes (25–29%) are dominant in the Slovakian samples (**Figure 4A**). The heavy minerals from the Slovakian sites are angular, subangular, less abraded showing short distance (<200 km) transportation. According to Nemec and Huraiová (2018), garnet and rutile minerals are from metamorphic source rocks and granitoid rocks. Probable provenance of these rock types includes underlying deep-seated intrusive igneous and

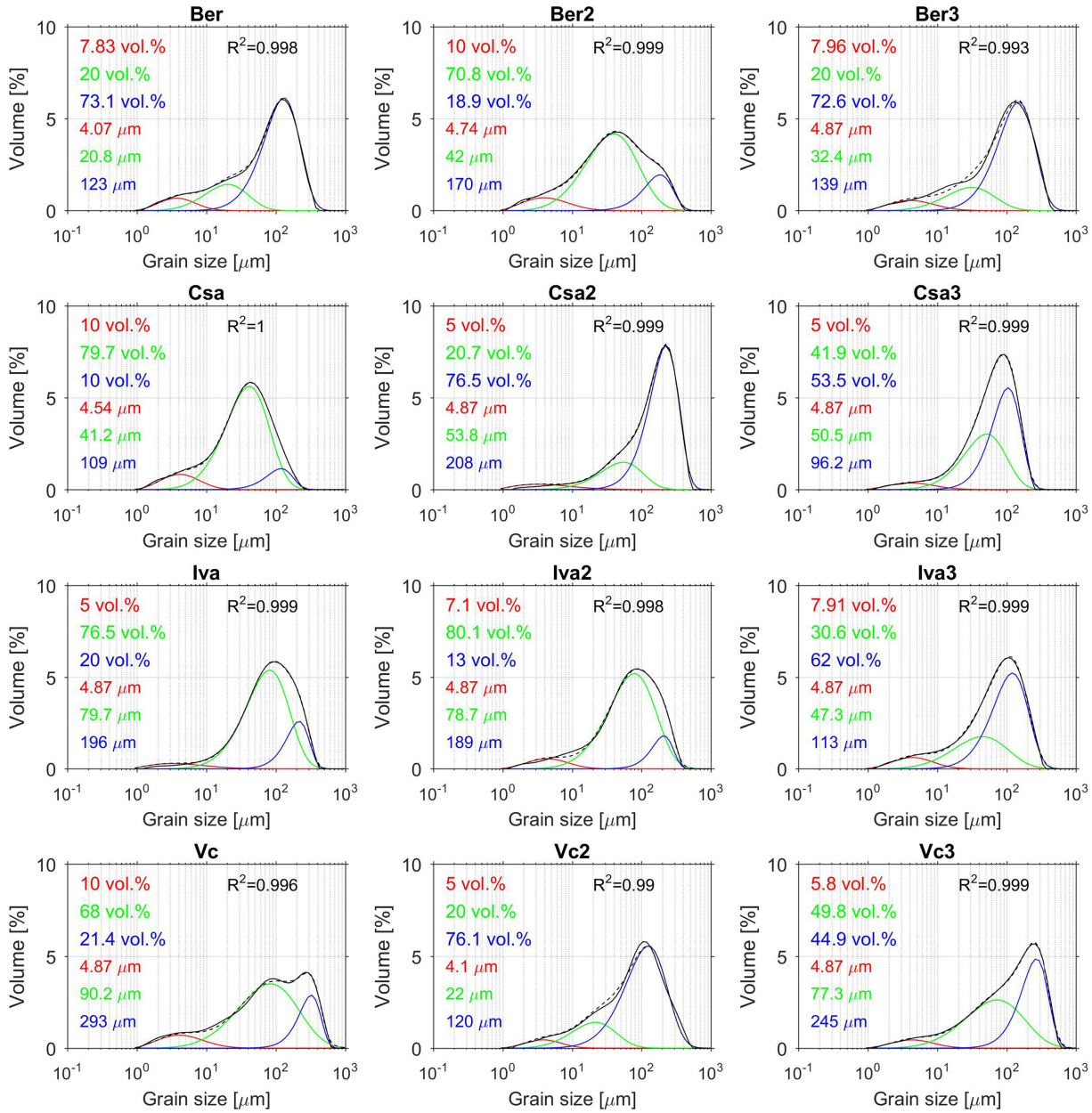

FIGURE 3 | Results of parametric curve-fitting of the measured grain-size distributions (volumetric amount and modal grain-sizes of the subpopulations are also presented). Three representative samples from the study sites are shown here. Ber, Beremend; Csa, Csarnóta; Iva, Ivanovce; Vc, Včeláre.

metamorphic basement formations or shallow basin watershed sediments transported from the Central Carpathians (Nemec and Huraiová, 2018). Certain garnet minerals may also be associated with granitic host rocks that appear as gravels in Paleogene-Neogene siliciclastics (Hurai et al., 2012; Nemec and Huraiová, 2018; Paquette et al., 2019). Garnet (21–23%), amphibole (26–27%), and epidote (25–27%) are dominant in the Hungarian samples (**Figure 4B**). Heavy minerals from these sites are abraded and well-rounded indicating a longer distance (>500 km) transportation. The River Danube from its catchment area transports garnet-dominated heavy mineral assemblages primarily from the Alps, and the Bohemian Massif (Grosz et al., 1985; Thamó-Bozsó and Juhász, 2002). The higher concentration of amphiboles in the samples indicates an additional hinterland. The Neogene calc-alkaline volcanic rocks from the Western Carpathians are likely the primary source for amphiboles (Thamó-Bozsó and Kovács, 2007).

Eolian Origin and Provenance

Although, it has already shown that the red clay sediments in karstified fissures are wind-blow in origin, but the whole processes require more observations due to the karst environment. Hypogene karstification has been reported from Hungary (Leél-Ossy, 2017; Mádl-Szonyi et al., 2017) and

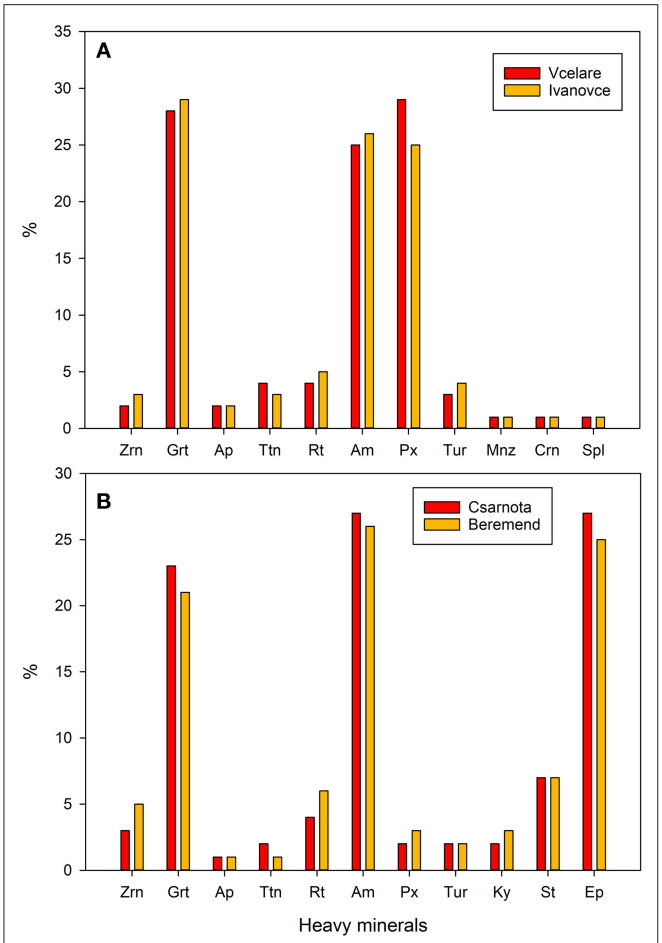

FIGURE 4 | Heavy mineral assemblages from Slovakia **(A)** and Hungary **(B)**. Zrn, zircon; Grt, garnet; Ap, apatite; Ttn, titanite; Rt, rutile; Am, amphibole; Px, pyroxene; Tur, tourmaline; Ky, kyanite; St, staurolite; Ep, epidote; Mnz, monazite; Crn, corundum; Spl, spinel.

especially from the region of Beremend (Erőss et al., 2020). It is important to be able to distinguish between allochthonous fissure filling sediments and ghost-rock (Dubois et al., 2014; Osborne, 2017; *in-situ* weathered rock, also called phantom rock). During ghost-rock karstification processes the interstitial flow through the fissure removes the more soluble ions while the less soluble residual minerals remain in place (Dubois et al., 2014). Fissure filling sediments are disconformable with the host limestone while ghost-rock is conformable with limestone containing host limestone structures and textures (Osborne, 2017). In our case, there is a sharp contrast (disconformable) between the fissure filling red sediments and the host rock. In the last two decades comprehensive granulometric analyses were made on the red silty clays and the overlying loess-paleosol successions in the Carpathian Basin (Kovács, 2008; Kovács et al., 2008, 2011, 2013; Újvári et al., 2010, 2016; Varga et al., 2012, 2016, 2018, 2019) These red clays show similarity in terms of their bimodal particle-size distribution patterns with loess horizons (Kovács et al., 2008, 2011). The fine dust ($<2\,\mu m$) could be represented in the fine component of the red clays. The source area of these fines (clay- and fine silt-sized) could be linked to the North African dust hot spots. As highlighted by Varga (2020), since 1979, ∼218 Saharan dust events have been observed in the Carpathian Basin. Based on this, we suggest that North African dust admixtures to red clays are likely, albeit with a very low (5–10%) contribution.

CONCLUSIONS

Multi-proxy formal analyses provide deeper insight into red paleosol genesis and material provenance situated in karstified fissures in Mesozoic limestones. This study demonstrates the presence of eolian sedimentation in paleokarst fissures located in the Carpathian Basin. Major characteristics of the grain-size distribution properties of wind-blown dust deposits are represented reasonably well by all applied procedures such as laser diffraction, high-resolution thin-section, and heavy mineral analyses. The mean grain size of the samples is definitely finer than eolian sand and coarser than Asian mineral dust but is akin to silt. Moreover, evidence that the eolian fissure sediments of Pliocene and Early Pleistocene age in the Triassic–Cretaceous limestones are derived from wind-driven red silt and clay includes compositional and textural analogs; especially granulometric trends detected downwards from the paleo-surface of the former landscape. The dust was derived from a combination of local (Slovakian sites) and longer-distance source areas (Hungarian sites), including hinterland located >500 km away from the study site. The heavy mineral assemblage indicates a very mature parent rock. The source of the red silty clay can be attributed to the alluvium and the wide riverbeds, the drainage basins of the Alps and the Western/Central Carpathians. Our study demonstrates that to develop a full granulometric report, joint methodology-system of parametric curve-fitting and RADIUS analyses are suggested. General vertical, bottom-up coarsening of the grain-size values of the fissure-filling sediments is clearly pointed-out by all of the investigated granulometric descriptors, indicators, and proxies. We report on the first time from Central Europe evidence for eolian sediments captured in paleokarst fissures and characterize the depositional signature of the red silty sediments using a novel integration of petrographic and granulometric techniques. These analyses enable us to specify the depositional process in an entirely diverse environment. Thus, our discovery provides a methodological framework for future characterization of eolian processes. This discovery is inherently interdisciplinary and is relevant to research into geomorphology, sedimentology, and atmospheric sciences.

DATA AVAILABILITY STATEMENT

The raw data supporting the conclusions of this article will be made available by the authors, without undue reservation.

AUTHOR'S NOTE

The preliminary results of this paper were published as a one-page abstract in the conference abstract book of the International Meeting of Sedimentology 2017—Toulouse, 10-12 October 2017.

AUTHOR CONTRIBUTIONS

JK and GÚ conceived the idea, performed the experiment, and conducted the analysis. JK, NG, and PS measured the grain size and GV and GÚ contributed to the analysis. JD provided the thin-sections and KS contributed to data interpretation. JK drafted the paper, with contributions from all co-authors.

FUNDING

The project has been supported by the European Union, co-financed by the European Social Fund: EFOP-3.6.1.-16-2016-00004 and the National Research, Development and Innovation Fund: NKFI K120213 and K120620.

ACKNOWLEDGMENTS

The authors are grateful to M. Sabol (Department of Geological and Paleontology, Comenius University in Bratislava, Slovakia) for supplying some additional sediment samples from the Slovakian sites. We are also grateful for the insightful comments offered by the peer reviewers.

REFERENCES

Al-Farraj, A., Slabe, T., Knez, M., Gabrovšek, F., Mulec, J., Petrič, M., et al. (2014). Karst in ras al-khaimah, Northern United Arab Emirates. *Acta Carsol.* 43, 23–42. doi: 10.3986/ac.v43i1.579

Andreucci, S., Sechi, D., Buylaert, J. P., Sanna, L., and Pascucci, V. (2017). Post-IR IRSL290 dating of K-rich feldspar sand grains in a wind-dominated system on Sardinia. *Mar. Pet. Geol.* 87, 91–98. doi: 10.1016/j.marpetgeo.2017.03.025

Atalay, I. (1997). Red Mediterranean soils in some karstic regions of Taurus Mountains, Turkey. *CATENA* 28, 247–260. doi: 10.1016/S0341-8162(96)00041-0

Bal, L., and Buursink, J. (1976). An Inceptisol formed in calcareous loess on the "Dast-i-Esan Top" plain in Afghanistan: fabric, mineral, and trace element analysis. *Neth. J. Agri. Sci.* 24, 17–42.

Bosák, P., and Zupan Hajna, N. (2018). Palygorskite in caves and karsts: a review. *Acta Carsol.* 47, 97–108. doi: 10.3986/ac.v47i2-3.5186

Bosch, R. F., and White, W. B. (2007). "Lithofacies and transport of clastic sediments in karstic aquifers," in *Studies of Cave Sediments: Physical and Chemical Records of Paleoclimate*, eds I. D. Sasowsky, and J. Mylroie (Dordrecht: Springer Netherlands), 1–22.

Bronger, A., Ensling, J., and Kalk, E. (1984). Mineralverwitterung, tonmineralbildung und rubefizierung in Terrae calcis der slowakei Ein beitrag zum paläoklimatischen aussagewert von kalkstein-Rotlehmen in Mitteleuropa. *Catena* 11, 115–132. doi: 10.1016/0341-8162(84)90002-X

Buggle, B., Glaser, B., Zöller, L., Hambach, U., Marković, S., Glaser, I., et al. (2008). Geochemical characterization and origin of Southeastern and Eastern European loesses (Serbia, Romania, Ukraine). *Quat. Sci. Rev.* 27, 1058–1075. doi: 10.1016/j.quascirev.2008.01.018

Costantini, E. A. C., Priori, S., Urban, B., Hilgers, A., Sauer, D., Protano, G., et al. (2009). Multidisciplinary characterization of the middle Holocene eolian deposits of the Elsa River basin (central Italy). *Quat. Int.* 209, 107–130. doi: 10.1016/j.quaint.2009.02.025

Coude-Gaussen, G., Rognon, P., and Fedoroff, N. (1984). Piégeage de poussières éoliennes dans des fissures de granitoïdes du Sinaï oriental. *C. R. Acad. Sci. Serie II* 298, 369–374.

Császár, G. (2002). Urgon formations in Hungary. *Geol. Hung. Ser. Geol.* 25, 1–208.

Dubois, C., Quinif, Y., Baele, J. M., Barriquand, L., Bini, A., Bruxelles, L., et al. (2014). The process of ghost-rock karstification and its role in the formation of cave systems. *Earth-Sci. Rev.* 131, 116–148. doi: 10.1016/j.earscirev.2014.01.006

Durn, G., Wacha, L., Bartolin, M., Rolf, C., Frechen, M., Tsukamoto, S., et al. (2018). Provenance and formation of the red palaeosol and lithified terra rossa-like infillings on the Island of Susak: a high-resolution and chronological approach. *Quat. Int.* 494, 105–129. doi: 10.1016/j.quaint.2017.11.040

Erőss, A., Csondor, K., Czuppon, G., Dezső, J., and Müller, I. (2020). Groundwater flow system understanding of the lukewarm springs in Kistapolca (South Hungary) and its relevance to hypogene cave formation. *Environ. Earth Sci.* 79:132. doi: 10.1007/s12665-020-8870-3

Evans, J. E., and Reed, J. M. (2007). Integrated loessite-paleokarst depositional system, early Pennsylvanian molas formation, Paradox Basin, southwestern Colorado, USA. *Sediment. Geol.* 195, 161–181. doi: 10.1016/j.sedgeo.2006.07.010

Evans, J. E., and Soreghan, M. (2015). Long-distance sediment transport and episodic resedimentation of Pennsylvanian dust (eolian silt) in cave passages of the Mississippian Leadville Limestone, southwestern Colorado, USA. *Geol. Soc. Am. Spec. Pap.* 516, 263–283. doi: 10.1130/2015.2516(21)

Fejfar, O. (1961). Die plio-pleistozänen wirbeltierfaunen von hajnácka und ivanovce (Slowakei), CSR. I. die fundumstände und stratigraphie. *Neues Jahrb. Geol. Paläontol.* 111, 257–273.

Fejfar, O., and Horáček, I. (1983). Zur entwicklung der kleinsäugerfaunen im villányium und altbiha rium auf dem gebiet der CSSR. *Schr. Reihe Geol. Wiss.* 19-20, 111–207.

Fejfar, O., Sabol, M., and Tóth, C. (2012). Early pliocene vertebrates from ivanovce and Hajnáčka (Slovakia). VIII. ursidae, mustelidae, tapiridae, bovidae and proboscidea from ivanovce. *Neues Jahrb. Geol. Paläontol.* 264, 95–115. doi: 10.1127/0077-7749/2012/0231

Fekete, J. (2002). Physical and chemical features of red clays in Northern Hungary. *Acta Geol. Hung.* 45, 231–246. doi: 10.1556/AGeol.45.2002.3.3

Fekete, J. (2014). Data to genetics of fossil red soils in Hungary. *Tájökológiai Lapok* 12, 117–125.

Ge, J., Deng, C., Wang, Y., Shao, Q., Zhou, X., Xing, S., et al. (2020). Climate-influenced cave deposition and human occupation during the Pleistocene in Zhiren Cave, southwest China. *Quat. Int.* doi: 10.1016/j.quaint.2020.01.018

Gil, H., Luzón, A., Soriano, M. A., Casado, I., Pérez, A., Yuste, A., et al. (2013). Stratigraphic architecture of alluvial–aeolian systems developed on active karst terrains: an early pleistocene example from the Ebro basin (NE Spain). *Sed. Geol.* 296, 122–141. doi: 10.1016/j.sedgeo.2013.08.009

Grosz, A. E., Rónai, A., and Lopez, R. (1985). Contribution to the determination of the Plio-Pleistocene boundary in sediments of the Pannonian Basin. *Geophys. Trans.* 31, 89–99.

Hurai, V., Paquette, J. L., Huraiová M., and Sabol, M. (2012). U–Pb geochronology of zircons from fossiliferous sediments of the Hajnácka I maar (Slovakia) – type locality of the MN16a biostratigraphic subzone. *Geol. Mag.* 149, 989–1000. doi: 10.1017/S0016756812000106

Jánossy, D. (1986). *Pleistocene Vertebrate Faunas of Hungary*. Amsterdam: Elsevier.

Kok, J. F., Parteli, E. J. R., Michaels, T. I., and Karam, B. D. (2012). The physics of wind-blown sand and dust. *Rep. Prog. Phys.* 75:106901. doi: 10.1088/0034-4885/75/10/106901

Konert, M., and Vandenberghe, J. (1997). Comparison of laser grain size analysis with pipette and sieve analysis: a solution for the underestimation of the clay fraction. *Sedimentology* 44, 523–535. doi: 10.1046/j.1365-3091.1997.d01-38.x

Kovács, J. (2008). Grain-size analysis of the Neogene red clay formation in the Pannonian Basin. *Int. J. Earth. Sci.* 97, 171–178. doi: 10.1007/s00531-006-0150-2

Kovács, J., Varga, G., and Dezső, J. (2008). Comparative study on the late cenozoic red clay deposits from China and Central Europe (Hungary). *Geol. Q.* 52, 369–382.

Kovács, J., Fábián, S. T., Varga, G., Újvári, G., Varga, G., and Dezső, J. (2011). Plio-pleistocene red clay deposits in the Pannonian basin: a review. *Quat. Int.* 240, 35–43. doi: 10.1016/j.quaint.2010.12.013

Kovács, J., Újvári, G., Varga, G., Farics, É., Dezső, J., and Sabol, M. (2017). "Eolian fissure filling sediments of karstified limestones in the Carpathian Basin," in *33rd International Meeting of Sedimentology - 16ème Congrès Français de Sédimentologie: Toulouse*, 10-12 October 2017, Abstract book, vol. 1-2. p. 473.

Kovács, J., Raucsik, B., Varga, A., Újvári, G., Varga, G., and Ottner, F. (2013). Clay mineralogy of red clay deposits from the central Carpathian Basin (Hungary): implications for plio-pleistocene chemical weathering and palaeoclimate. *Turk. J. Earth Sci.* 22, 414–426. doi: 10.3906/yer-1201-4

Leél-Ossy, S. (2017). "Caves of the buda thermal karst," in *Hypogene Karst Regions and Caves of the World*, eds. A. Klimchouk, A. N. Palmer, J. De Waele, A. S. Auler, and P. Audra (Cham: Springer International Publishing), 279–297. doi: 10.1007/978-3-319-53348-3_18

Mádl-Szonyi, J., Erőss, A., and Tóth, Á. (2017). "Fluid flow systems and hypogene karst of the Transdanubian range, Hungary—with special emphasis on buda thermal karst," in *Hypogene Karst Regions and Caves of the World*, eds A. Klimchouk, A. N. Palmer, J. de Waele, A. S. Auler, and P. Audra (Cham: Springer International Publishing), 267–278.

Mange, M. A., and Maurer, H. F. W. (1992). *Heavy Minerals in Colour*. London, UK: Chapman & Hall.

Marković, S. B., Stevens, T., Kukla, G. J., Hambach, U., Fitzsimmons, K. E., Gibbard, P., et al. (2015). The danube loess stratigraphy – new steps towards the development of a pan-European loess stratigraphic model. *Earth Sci. Rev.* 148, 228–258. doi: 10.1016/j.earscirev.2015.06.005

Merino, E., and Banerjee, A. (2008). Terra rossa genesis, implications for karst, and eolian dust: a geodynamic thread. *J. Geol.* 116, 62–75. doi: 10.1086/524675

Mikulčić Pavlaković, S., Crnjaković, M., Tiljaš, D., Šoufek, M., Wacha, L., Frechen, M., et al. (2011). Mineralogical and geochemical characteristics of quaternary sediments from the Island of Susak (Northern Adriatic, Croatia). *Quat. Int.* 234, 32–49. doi: 10.1016/j.quaint.2010.02.005

Musgrave, R. J., and Webb, J. A. (2004). "Palaeomagnetic analysis of sediments in the buchan caves, Southeastern Australia, provides a prelate pleistocene date for landscape and climate evolution," in *Studies of Cave Sediments*, eds. I. D. Sasowsky and J. Mylroie (Boston, MA: Springer International Publishing), 47–69.

Muttoni, G., Sirakov, N., Guadelli, J. L., Kent, D. V., Scardia, G., Monesi, E., et al. (2017). An early Brunhes (<0.78 Ma) age for the Lower Paleolithic tool-bearing Kozarnika cave sediments, Bulgaria. *Quat. Sci. Rev.* 178, 1–13. doi: 10.1016/j.quascirev.2017.10.034

Nemec, O., and Huraiová, M. (2018). Provenance study of detrital garnets and rutiles from basaltic pyroclastic rocks of Southern Slovakia (*Western Carpathians*). *Geol. Carpath.* 69, 17–29. doi: 10.1515/geoca-2018-0002

Obreht, I., Zeeden, C., Hambach, U., Veres, D., Marković, S. B., and Lehmkuhl, F. (2019). A critical reevaluation of palaeoclimate proxy records from loess in the Carpathian Basin. *Earth Sci. Rev.* 190, 498–520. doi: 10.1016/j.earscirev.2019.01.020

Osborne, R. A. L. (2017). Palaeokarst deposits in caves: Examples from eastern Australia and central Europe. *Acta Carsol.* 46, 19–32. doi: 10.3986/ac.v46i1.4637

Paquette, J., Huraiová, M., Nemec, O., Gannoun, A., Sarinova, K., and Hurai, V. (2019). Origin and provenance of 2 Ma−2 Ga zircons ejected by phreatomagmatic eruptions of Pliocene basalts in southern Slovakia. *Int. J. Earth. Sci.* 108, 2607–2623. doi: 10.1007/s00531-019-01779-7

Pazonyi, P., Mészáros, L., Hír, J., and Szentesi, Z. (2016). The lowermost pleistocene rodent and soricid (Mammalia) fauna from Beremend 14 locality (South Hungary) and its biostratigraphical and palaeoecological implications. *Fragm. Pal. Hung.* 33, 99–134. doi: 10.17111/FragmPalHung.2016.33.99

Peng, X., Wang, X., Dai, Q., Ding, G., and Li, C. (2019). Soil structure and nutrient contents in underground fissures in a rock-mantled slope in the karst rocky desertification area. *Environ. Earth Sci.* 79:3. doi: 10.1007/s12665-019-8708-z

Peresani, M., Cremaschi, M., Ferraro, F., Falguères, C., Bahain, J. J., Gruppioni, G., et al. (2008). Age of the final Middle Palaeolithic and Uluzzian levels at Fumane Cave, Northern Italy, using ^{14}C, ESR, ^{234}U/^{230}Th and thermoluminescence methods. *J. Archaeol. Sci.* 35, 2986–2996. doi: 10.1016/j.jas.2008.06.013

Pickford, M., and Mein, P. (1988). The discovery of fossiliferous Plio-pleistocene cave fillings in Ngamiland, Botswana. *C. R. Acad. Sci. Ser. II* 307, 1681–1686.

Rellini, I., Firpo, M., Martino, G., Riel-Salvatore, J., and Maggi, R. (2013). Climate and environmental changes recognized by micromorphology in paleolithic deposits at Arene Candide (Liguria, Italy). *Quat. Int.* 315, 42–55. doi: 10.1016/j.quaint.2013.05.050

Sabol, M., Holec, P., and Wagner, J. (2008). Late pliocene carnivores from Včeláre 2 (Southeastern Slovakia). *Paleontol. J.* 42, 531–543. doi: 10.1134/S0031030108050092

Seelos, K., and Sirocko, F. (2005). RADIUS - rapid particle analysis of digital images by ultra-high-resolution scanning of thin sections. *Sedimentology* 52, 669–681. doi: 10.1111/j.1365-3091.2005.00715.x

Seelos, K., Sirocko, F., and Dietrich, S. (2009). A continuous high-resolution dust record for the reconstruction of wind systems in central Europe (Eifel, Western Germany) over the past 133 ka. *Geophys. Res. Lett.* 36:L20712. doi: 10.1029/2009GL039716

Sirocko, F., Seelos, K., Schaber, K., Rein, B., Dreher, F., Diehl, M., et al. (2005). A late Eemian aridity pulse in central Europe during the last glacial inception. *Nature* 436, 833–836. doi: 10.1038/nature03905

Smalley, I., O'Hara-Dhand, K., Wint, J., Machalett, B., Jary, Z., and Jefferson, I. (2009). Rivers and loess: the significance of long river transportation in the complex event-sequence approach to loess deposit formation. *Quat. Int.* 198, 7–18. doi: 10.1016/j.quaint.2008.06.009

Soriano, M. A., Pocoví, A., Gil, H., Perez, A., Luzón, A., and Marazuela, M. Á. (2019). Some evolutionary patterns of palaeokarst developed in pleistocene deposits (Ebro Basin, NE Spain): Improving geohazard awareness in present-day karst. *Geol. J.* 54, 333–350. doi: 10.1002/gj.3181

Stevens, T., Marković, S. B., Zech, M., Hambach, U., and Sümegi, P. (2011). Dust deposition and climate in the Carpathian Basin over an independently dated last glacial-interglacial cycle. *Quat. Sci. Rev.* 30, 662–681. doi: 10.1016/j.quascirev.2010.12.011

Sun, D., Bloemendal, J., Rea, D. K., An, Z., Vandenberghe, J., Lu, H., et al. (2004). Bimodal grain-size distribution of Chinese loess, and its paleoclimatic implications. *Catena* 55, 325–340. doi: 10.1016/S0341-8162(03)00109-7

Sun, D., Bloemendal, J., Rea, D. K., Vandenberghe, J., Jiang, F., An, Z., et al. (2002). Grain-size distribution function of polymodal sediments in hydraulic and aeolian environments, and numerical partitioning of the sedimentary components. *Sediment. Geol.* 152, 263–277. doi: 10.1016/S0037-0738(02)00082-9

Szentesi, Z., Pazonyi, P., and Mészáros, L. (2015). Albanerpetontidae from the late Pliocene (MN 16A) Csarnóta 3 locality (Villány Hills, South Hungary) in the collection of the Hungarian Natural History Museum. *Fragm. Pal. Hung.* 32, 49–66. doi: 10.17111/FragmPalHung.2015.32.49

Thamó-Bozsó, E., and Juhász, G. (2002). Mineral composition of upper miocene–pliocene (pannonian s.l.) sands and sandstones in the different sedimentary subbasins in Hungary. *Geol. Carpath.* 53, 1–6.

Thamó-Bozsó, E., and Kovács, L. Ó. (2007). Evolution of Quaternary modern fluvial network in the Mid-Hungarian plain, indicated by heavy mineral distributions and statistical analysis of heavy mineral data. *Dev. Sedimetol.* 58, 491–514. doi: 10.1016/S0070-4571(07)58019-2

Török, Á. (1998). Controls on development of Mid-Triassic ramps: examples from southern Hungary. *Geol. Soc. Spec. Publ.* 149, 339–367. doi: 10.1144/GSL.SP.1999.149.01.16

Tsoar, H., and Pye, K. (1987). Dust transport and the question of desert loess formation. *Sedimentology* 34, 139–153. doi: 10.1111/j.1365-3091.1987.tb00566.x

Újvári, G., Kok, J. F., Varga, G., and Kovács, J. (2016). The physics of wind-blown loess: Implications for grain size proxy interpretations in Quaternary paleoclimate studies. *Earth Sci. Rev.* 154, 247–278. doi: 10.1016/j.earscirev.2016.01.006

Újvári, G., Kovács J., Varga, G., Raucsik, B., and Markovic, S. B. (2010). Dust flux estimates for the Last Glacial Period in East Central Europe based on terrestrial records of loess deposits: a review. *Quat. Sci. Rev.* 29, 3157–3166. doi: 10.1016/j.quascirev.2010.07.005

Újvári, G., Varga, A., Ramos, F. C., Kovács, J., Németh, T., and Stevens, T. (2012). Evaluating the use of clay mineralogy, Sr–Nd isotopes and zircon U–Pb ages in tracking dust provenance: an example from loess of the Carpathian Basin. *Chem. Geol.* 304-305, 83–96. doi: 10.1016/j.chemgeo.2012.02.007

Vandenberghe, J. (2013). Grain size of fine-grained windblown sediment: a powerful proxy for process identification. *Earth Sci. Rev.* 121, 18–30. doi: 10.1016/j.earscirev.2013.03.001

Vandenberghe, J., Sun, Y., Wang, X., Abels, H. A., and Liu, X. (2018). Grain-size characterization of reworked fine-grained aeolian deposits. *Earth Sci. Rev.* 177, 43–52. doi: 10.1016/j.earscirev.2017.11.005

Varga, A., Újvári, G., and Raucsik, B. (2011). Tectonic versus climatic control on the evolution of a loess-paleosol sequence at Beremend, Hungary: an integrated approach based on paleoecological, clay mineralogical, and geochemical data. *Quat. Int.* 240, 71–86. doi: 10.1016/j.quaint.2010.10.032

Varga, G. (2020). Changing nature of Saharan dust deposition in the Carpathian Basin (Central Europe): 40 years of identified North African dust events (1979–2018). *Environ. Int.* 139:105712. doi: 10.1016/j.envint.2020.105712

Varga, G., Cserháti, C., Kovács, J., and Szalai, Z. (2016). Saharan dust deposition in the Carpathian Basin and its possible effects on interglacial soil formation. *Aeolian Res.* 22, 1–12. doi: 10.1016/j.aeolia.2016.05.004

Varga, G., Kovács, J., Szalai, Z., Cserháti, C., and Újvári, G. (2018). Granulometric characterization of paleosols in loess series by automated static image analysis. *Sediment. Geol.* 370, 1–14. doi: 10.1016/j.sedgeo.2018.04.001

Varga, G., Kovács, J., and Újvári, G. (2012). Late Pleistocene variations of the background aeolian dust concentration in the Carpathian Basin: an estimate using decomposition of grain-size distribution curves of loess deposits. *Geol. Mijnb./Neth. J. Geosci.* 91, 159–171. doi: 10.1017/S0016774600001566

Varga, G., Újvári, G., and Kovács, J. (2019). Interpretation of sedimentary (sub)populations extracted from grain size distributions of Central European loess-paleosol series. *Quat. Int.* 502, 60–70. doi: 10.1016/j.quaint.2017.09.021

Viczián, I. (2002). Clay mineralogy of Quaternary sediments covering Mountainous and hilly areas of Hungary. *Acta Geol. Hung.* 45, 265–286. doi: 10.1556/AGeol.45.2002.3.5

Viczián, I. (2011). Hungarian contribution to the mineralogy and geology of clays: commemorating the 50th anniversary of the Hungarian Clay Minerals Group founded in 1960. *Földt. Közl.* 141, 313–319.

Villa, N., Dorn, R. I., and Clark, J. (1995). "Fine material in rock fractures: Aeolian dust or weathering?," in *Desert Aeolian Processes,* ed. V. P. Tchakerian (Dordrecht: Springer Netherlands), 219–231.

Conflict of Interest: The authors declare that the research was conducted in the absence of any commercial or financial relationships that could be construed as a potential conflict of interest.